Bulletin of the Seismological Society of America, Vol. 94, No. 4, pp. 1456–1466, August 2004

Application of Autoregressive Extrapolation to Seismic Tomography

by Cuiping Li and Robert L. Nowack

Abstract Seismic tomography used in the laboratory, as well as in the field, is strongly affected by limited and nonuniform ray coverage. A two-stage autoregressive extrapolation technique is proposed that can be used to extend the observed data and provide better tomographic images. The algorithm is based on the principle that the extrapolated data add minimal information to the existing data. The first stage of the extrapolation is to find the optimal prediction-error (PE) filter. The second stage is to use the PE filter to find the values of the missing data. The missing data are estimated to have the same spectrum as the observed data and are similar to maximizing an entropy criterion. To test the method, synthetic tomography experiments for laboratory rock samples are used in which full ray coverage can be obtained. Autoregressive methods are then used to extrapolate the partial ray coverage and the tomographic results are compared with the full ray coverage case. The synthetic tests show that the autoregressive method can extrapolate known data to find missing data and can provide improved tomographic images. The autoregressive extrapolation is also tolerant to noise. Although the method was applied to a laboratory geometry where the ray coverage can be controlled, autoregressive methods may have important applications to tomography experiments in the field where complete ray coverage often cannot be easily realized.

Introduction

Autoregressive extrapolation methods have been used in signal processing to predict time series and to perform prediction-error filtering. These methods can also be used to replace missing or corrupted samples and have been used in image processing and audio signal restoration (Jain, 1989; Goodsill and Rayner, 1998). Claerbout (1992, 2003) and Fomel and Claerbout (2003) suggested a two-stage approach to apply autoregressive techniques to linear geophysical inverse problems. The first stage is to find the optimal prediction-error (PE) filter. The second stage is to assume that the PE filter is known and to estimate the missing data. Autoregressive signal-analysis techniques are often applied in one dimension, whereas seismic experiments are usually multidimensional. To overcome this difficulty, a helical coordinate system has been developed (Claerbout, 1998).

A common problem in seismic experiments is that the coverage of the acquired data is not large enough for complete geophysical structure reconstructions (Fomel, 2003a,b). To fully utilize the observed data, a method is needed to extrapolate the available data beyond the measurement range where the extrapolated data are required to add minimum information to the existing data. This is similar to maximizing an entropy criterion (Burg, 1975). The PE filter has this property, and its output tends to be white when the limit of the filter size goes to infinity (Claerbout, 1992).

In this article, we investigate the application of autoregressive methods to seismic tomography problems. We propose and implement a data extrapolation method based on Claerbout's approach for performing seismic data prediction beyond the measurement range. The idea of our algorithm is that the useful information in the known data is relevant and can be used to estimate the missing values by autoregressive extrapolation methods, and the estimated data only add minimum information to the known data. We apply this algorithm to synthetic arrival time data, with and without random noise added, and also to real laboratory experimental data. The results show that the proposed technique can extrapolate seismic travel-time data for seismic tomography, and the method is tolerant to random noise in the data.

Autoregressive Methods

Autoregressive (AR) methods can be used for prediction and extrapolation and have found wide applications in a number of fields (Jain, 1989; Goodsill and Rayner, 1998). Unlike many extrapolation techniques, AR methods are stochastic and take advantage of the statistics of the data. An autoregressive process of order p is a zero-mean random sequence y_i that uses the most recent p outputs and the current input to generate recursively the next output (Jain, 1989). The autoregressive process of order p has the form

$$y_i = \sum_{k=1}^{p} g_k y_{i-k} + \varepsilon_i, \tag{1}$$

where g_k are elements of the PE filter F and ε_i is a zero-mean input sequence that is independent of past outputs. The quantity

$$\bar{y}_i \approx \sum_{k=1}^{p} g_k y_{i-k} \tag{2}$$

is the best linear mean-square predictor of y_i based only on the previous p samples. From equations (1) and (2) we get

$$y_i = \bar{y}_i + \varepsilon_i, \tag{3}$$

which says that the value at sample i is the sum of its prediction estimate plus the prediction error ε_i.

Autoregressive extrapolation methods were originally used in signal processing to predict time series and to perform PE filtering. As an example for $p = 2$, given y_{i-1} and y_{i-2}, then y_i can be predicted using an autoregressive model. The prediction would be a scaled sum of y_{i-1} and y_{i-2}. The following equations would then need to be solved to find the prediction filter (g_1, g_2):

$$\begin{pmatrix} y_2 \\ y_3 \\ y_4 \\ y_5 \\ y_6 \end{pmatrix} = \begin{pmatrix} y_1 & y_0 \\ y_2 & y_1 \\ y_3 & y_2 \\ y_4 & y_3 \\ y_5 & y_4 \end{pmatrix} \begin{pmatrix} g_1 \\ g_2 \end{pmatrix}. \tag{4}$$

AR extrapolation methods can also be used to replace missing and corrupted samples with estimates of their true values. As applied to data extrapolation, Claerbout (1998) and Fomel and Claerbout (2003) suggested a two-stage process and the concept of a helix filter to overcome the boundary condition limitations for multidimensional extrapolation.

Two-Stage Data Extrapolation

The two-stage AR extrapolation approach can be used to apply autoregressive techniques to the linear least-squares problem. The first stage is to find the optimal PE filter. The second stage is to find the missing data assuming that the PE filter is known. The output of the PE filter tends to be white and the missing data values are estimated with the same spectrum as the known data. This is similar to maximizing an entropy criterion (Burg, 1975).

A geophysical inverse problem with both missing data and an unknown PE filter can be written as

$$\mathbf{A}x - \begin{bmatrix} y_a \\ y_b \end{bmatrix} = r_1 \approx 0 \tag{5a}$$

and

$$\mathbf{F}\begin{bmatrix} y_a \\ y_b \end{bmatrix} = r_2 \approx 0, \tag{5b}$$

In the first equation the model parameters x are related to the data by the sensitivity matrix $\mathbf{A}$, y_a are the known data, and y_b are the unknown data. Setting $r_1 \approx 0$ is equivalent to minimizing the data residuals. Using an L_2 norm, this results in the best-fitting model that minimizes the residuals in a least-squares sense. In the second equation the unknown data y_b are related to known data y_a by the PE filter $\mathbf{F}$. Setting $r_2 \approx 0$ means that we want to find y_b from y_a that minimizes this fitting goal.

We can constrain the PE filter $\mathbf{F}$ to be of the form (1, $f_1, f_2, \ldots, f_k$). As an example, for a three-term filter, equation (4) can be written with $f_1 = -g_1$ and $f_2 = -g_2$ as

$$\begin{bmatrix} y_1 & 0 & 0 \\ y_2 & y_1 & 0 \\ y_3 & y_2 & y_1 \\ y_4 & y_3 & y_2 \\ y_5 & y_4 & y_3 \\ 0 & y_5 & y_4 \\ 0 & 0 & y_5 \end{bmatrix} \begin{pmatrix} 1 \\ f_1 \\ f_2 \end{pmatrix} \approx 0, \tag{6}$$

assuming $y_{-1} = y_0 = 0$ and $y_6 = y_7 = 0$. This can also be written in an alternate convolutional form similar to equation (5b) as

$$\begin{bmatrix} 1 & 0 & 0 & 0 & 0 \\ f_1 & 1 & 0 & 0 & 0 \\ f_2 & f_1 & 1 & 0 & 0 \\ 0 & f_2 & f_1 & 1 & 0 \\ 0 & 0 & f_2 & f_1 & 1 \\ 0 & 0 & 0 & f_2 & f_1 \\ 0 & 0 & 0 & 0 & f_2 \end{bmatrix} \begin{pmatrix} y_1 \\ y_2 \\ y_3 \\ y_4 \\ y_5 \end{pmatrix} \approx 0. \tag{7}$$

We can solve the nonlinear problem of estimating $\mathbf{F}$ and y using a linearized iterative approach (VanDecar and Snieder, 1994). We first need a starting guess $\mathbf{F_0}$ for $\mathbf{F}$. Then we can use $\mathbf{F_0}$ to get y_0, and then use y_0 to get $\mathbf{F_1}$, etc., and iteratively solve this until we get convergence.

We can then write (5a) and (5b) as

$$\begin{bmatrix} \mathbf{A_a} \\ \mathbf{A_b} \end{bmatrix} x \approx \begin{bmatrix} y_a \\ y'_b \end{bmatrix} \tag{8}$$

where y'_b is the autoregressive extrapolation of y_b given y_a. This is a special form of the regularized geophysical inverse problem.

We can apply the AR technique to the seismic tomography inverse problem in several alternative ways. In terms of estimating model parameters we could do the following:

1. Remove those model pixels with few or no rays from the inversion, and invert only for pixels with good ray coverage.

2. Make use of the inversion result from step 1 and incorporate the AR interpolation technique to the model to get the values for those pixels left out.

In terms of insufficient data we could apply the AR technique directly to the missing data as follows:

1. Extrapolate the data from the known data to the unknown data.
2. Tomographically invert the combined known and extrapolated data for the model parameters.

In this article we will investigate the second approach. For the examples we use in rock mechanics, the changing pattern in the tomographic data may be more predictable and clearer than the estimated model parameters. Applying AR extrapolation techniques to the model space would require a heavily damped system to stabilize the incomplete tomographic system. This would then affect all the nodes of the model. An autoregressive extrapolation in the model space would then need to also correct for the damping imposed. Applying the AR extrapolation in the data space avoids this additional complication.

These ideas can be extended to multidimensions. For 2D AR extrapolation the input data and output data are arrays of numbers and the PE filter is also an array. A 2D PE filter is a small array that is convolved over a larger data array. For example, a 2D 3 by 3 PE filter can be constrained to have the following form:

$$\begin{pmatrix} 0 & b & e \\ 1 & c & f \\ a & d & g \end{pmatrix}, \tag{9}$$

where the leading 1 is the constrained coefficient and (a, b, c, d, e, f, g) are the free coefficients. The free coefficients are first set to initial values as input to the filter estimation process. To find the PE filter, the data are assumed to be known. After computing the PE filter, we can estimate the missing data.

The Helix Filter

Autoregressive analysis is one of the most powerful signal-analysis techniques. Although it has often been used in 1D problems, most geophysical experiments are multidimensional. To apply 1D AR techniques to multidimensional geophysical problems, Claerbout (1998) proposed the concept of a helical filter. The basic principle for this concept is that multidimensional data can be analyzed effectively as being one dimensional. Helical coordinates make it possible to do the multidimensional data extrapolation using a 1D algorithm. The trick is that a data set in multidimensional space can be unwrapped into a 1D data set and then a 1D AR algorithm can be applied to do the data extrapolation.

Unwrapping a multidimensional data set into a 1D data set creates a helix (Claerbout, 1998, 2003; Fomel and Claerbout, 2003). After the original 2D data set is unwrapped into its 1D equivalent form, multidimensional convolution can then be done with a 1D convolution program. After unwrapping the multidimensional data set into a 1D strip, a multidimensional convolution is then equivalent to a 1D convolution with a long 1D filter with internal gaps. During the helical convolution the gaps are simply skipped and by applying the appropriate helical boundary condition a multidimensional filter is mapped to its 1D equivalent (Fomel and Claerbout, 2003).

Using a helix filter is not really beneficial to the convolution process because convolution can be conducted in any order. The benefit of using the helix filter lies in the performance of deconvolution in a multidimensional space. Because deconvolution undoes convolution by taking the past outputs as its inputs and recursively filtering, it must be done sequentially; namely, it only can be done one dimensionally (Claerbout 1998 Formel and Clearbout, 2003). However, the helix filter allows one to apply deconvolution to a multidimensional space by changing the multidimensional space into an equivalent 1D space.

Applications

In seismic tomography, the parameters of the model can be correctly estimated only if we have adequate and uniform ray coverage. The lack of uniform ray coverage will result in some blocks having more rays and some blocks having fewer or no rays. This is related to the source and receiver geometry and will significantly affect the tomographic results. To show the effect of nonuniform ray coverage on

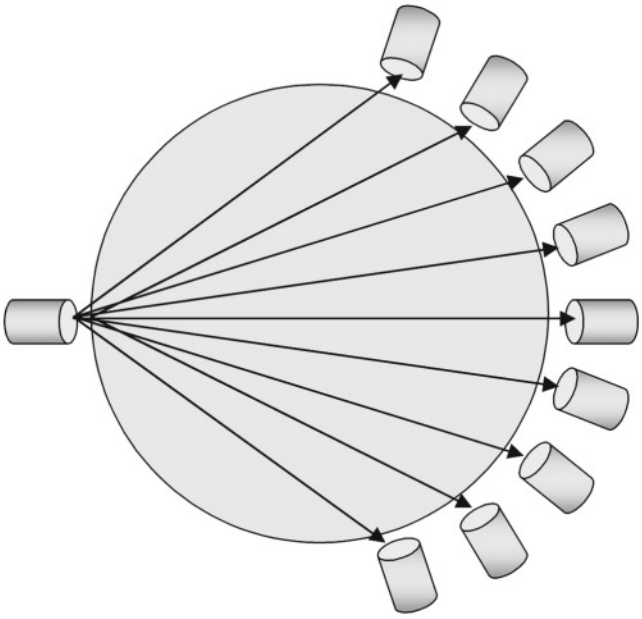

Figure 1. An example of one source and its receiver geometry. The transmitted signals are recorded at their corresponding receiver position for each source.

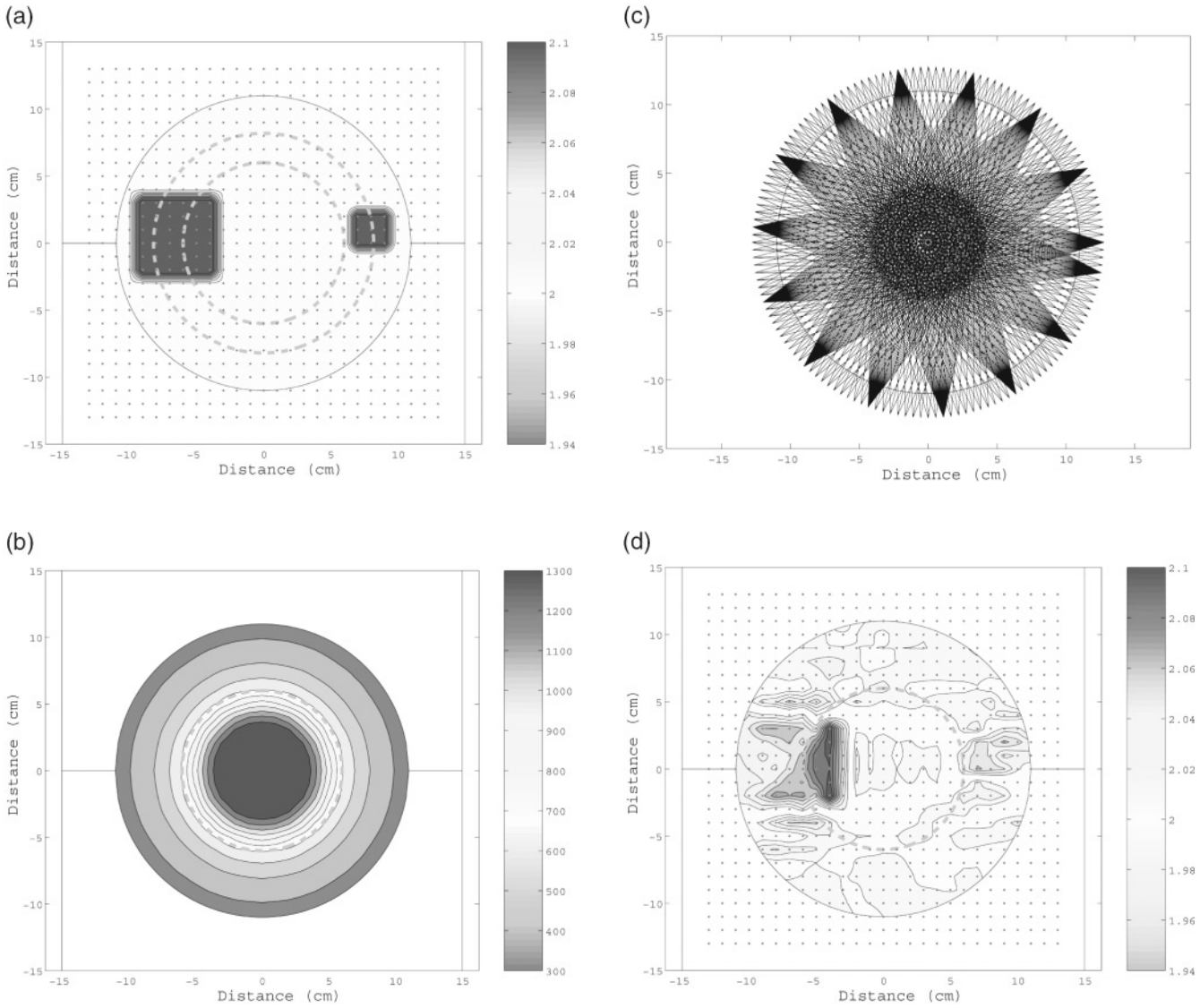

Figure 2. Synthetic inversion (with the rotation of the receivers spanning a 70-degree arc). (a) The true model. (b) Ray density plot. (c) Ray diagram for every 10 source positions. (d) Inversion result using simple damping. The dashed circles show the regions of higher ray density.

tomographic results, synthetic travel-time data sets have been produced and used to do tomographic reconstructions. We used a ray geometry for a tomographic experiment of a rock sample in the laboratory for which complete ray coverage is possible. Rays are then removed to get partial ray coverage. Figure 1 shows an example of one source and its corresponding receiver geometry. These examples use 135 total sources that are distributed around a cylindrial model. All the sources have the same separation to the edge of the model, and the angular distance between each pair of consecutive sources is 2.5 degrees. For each source there are a number of receivers that record the travel times, and the angular separation between each pair of consecutive receivers is also 2.5 degrees.

The initial synthetic examples use two data sets with partial ray coverage. The first data set has less angular ray coverage than the second one and has 29 receivers for each source point spanning a 70-degree arc. The second data set has 41 receivers for each source point spanning a 100-degree arc. Both cases have denser ray coverage at the center of the model and sparser ray coverage near the edges. The true model is shown in Figure 2a, where there are two high-velocity heterogeneities with $v = 2.1$ km/s embedded in a homogeneous background of $v = 2.0$ km/s. Figure 2b is a ray density plot for the first data set, where the dashed circle encloses the region of higher ray coverage. Figure 2c is a ray diagram plot for every 10 source positions and shows that the ray distribution is highly nonuniform with higher ray coverage at the center part of the model and fewer rays at the edges. Figure 2d is the tomographic inversion result

using simple damping. The model is seen to be properly inverted within the dashed circle enclosing the region of higher ray coverage. In the region of lower ray coverage the tomographic results are significantly degraded.

Figure 3 shows the results for the second data set, where the true model is shown in Figure 2a. Figure 3a, b, and c are the ray density plot, ray diagram for every 10 source positions, and inversion result with simple damping, respectively. Comparing Figure 3a and b to Figure 2b and c, we can see that the second data set has a larger region of denser ray coverage. The difference between the ray coverage has an important effect on the tomographic inversion results as shown in Figure 2d and 3c. Figure 3c shows a significant improvement compared to Figure 2d because of the increased region of higher ray coveraged.

In a similar fashion, for real tomography experiments in the laboratory and in the field, the data may not cover a large enough area or may be highly nonuniform, and this will severely affect the reconstruction results. We will next show several synthetic tomographic examples and one real data example to see how well the two-stage AR extrapolation technique works for tomographic problems using a laboratory geometry.

Synthetic Tomographic Example Without Noise

The two-stage AR extrapolation technique is now applied to synthetic tomographic data sets for a laboratory geometry. The source–receiver geometry is the same as shown in Figure 1. For each source position, 65 receivers now span a 160-degree arc around the sample and there is a 2.5-degree separation between every two contiguous receivers as well as sources. Rays have been traced from each source to its corresponding receivers for both the synthetic true model shown in Figure 4 and a homogenous background starting model, and the travel times are computed. The velocity of the heterogeneities is 2.1 km/s and the homogeneous background velocity is 2.0 km/s. Figure 5a is a common midpoint plot of the travel-time differences between the inhomoge-

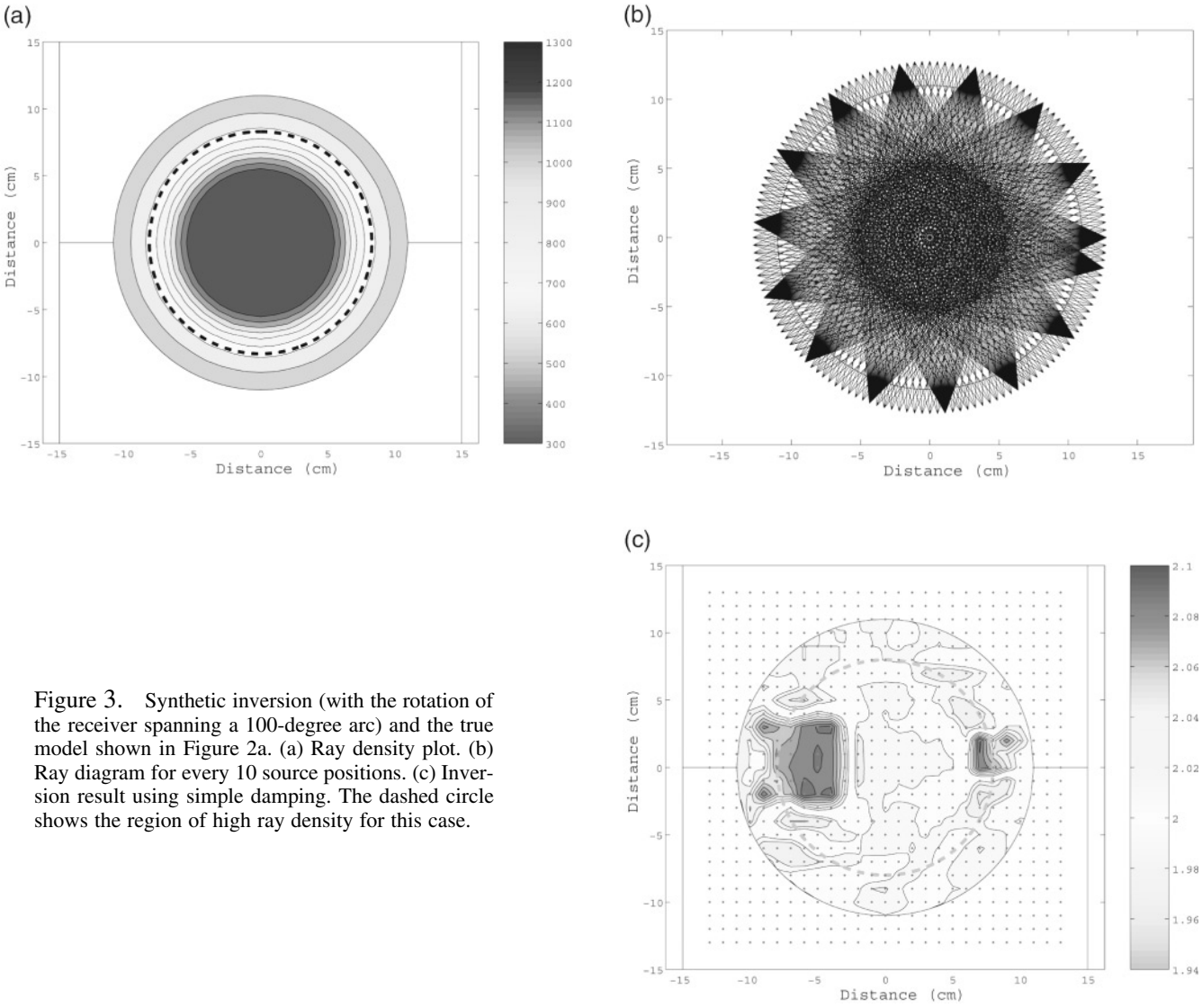

Figure 3. Synthetic inversion (with the rotation of the receiver spanning a 100-degree arc) and the true model shown in Figure 2a. (a) Ray density plot. (b) Ray diagram for every 10 source positions. (c) Inversion result using simple damping. The dashed circle shows the region of high ray density for this case.

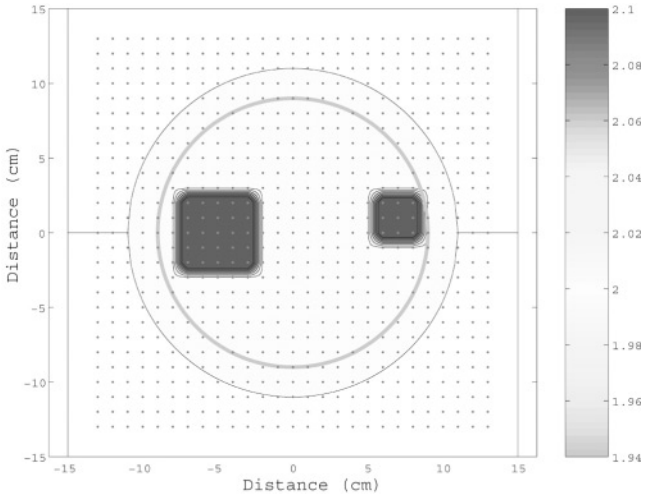

Figure 4. Synthetic true model used to generate synthetic travel-time data.

neous true model shown in Figure 4 and the homogeneous background starting model for 160-degree receiver-spanning arcs. Removing 40 degrees from each side of the data in Figure 5a results in the reduced data in Figure 5b with 80-degree receiver-spanning arcs.

A two-stage AR technique is used to extend the travel-time data for the receiver arcs spanning 80 degrees in Figure 5b to extrapolated 160-degree receiver spanning arcs. We chose a 2D 9 by 7 PE filter for our AR extrapolation, which has a similar form to equation (9). First, the 2D data and filter are unwrapped into their 1D equivalent forms. Then, we iteratively solve equations (6) and (7) until the results converge. The extended data result shown in Figure 5c can be seen to have the same overall patterns as the true data in Figure 5a. The data sets shown in Figure 5a, b, and c are then used for damped tomographic inversion (Tarontola, 1987; Wang, 1993). The damping tomographic inversion used in this example is

$$\Delta v = (A^*A + \alpha C_{x_0}^{-1} + \beta I)^{-1} A^*\Delta t, \qquad (10)$$

where A is the sensitivity matrix, $C_{x_0}^{-1}$ is the inverse of a prior model covariance matrix, Δt is the data residual, α and β are the damping coefficients, and Δv is the velocity perturbation to the model. The chosen values of α and β result from tests run to obtain the best trade-off between the damping and smoothing of the model inversion results and the fit to the data. The chosen values for α and β were then used for all the reconstructions in the synthetic and real data examples. Figure 6a is the tomographic inversion result using the full data set for 160-degree receiver spanning arcs in Figure 5a. Figure 6b shows the tomographic inversion result for the data set of 80-degree receiver spanning arcs in Figure 5b that is disgraded at the edges of the heterogeneities outside the circle of higher ray coverage shown by the solid circle in Figure 6. Figure 6c is the plot of the inversion using the extended data in Figure 5c. Comparing the inversion result shown in Figure 6c to those in Figure 6a and b, we see that the tomographic inversion result using the extended data shows a large improvement compared to the result shown in Figure 6b and is very close to the inversion using the entire data set shown in Figure 5a.

Both the plots for travel-time differences and the tomographic inversion results show that for our synthetic tomography test of the AR extrapolation technique has effectively extended the travel-time data from the 80-degree spanning arcs to the 160-degree spanning arcs and the inversion result using the extended data has been greatly improved.

Synthetic Tomographic Testing with Random Noise

To test the performance of the AR extrapolation technique with noisy data, normally distributed random noise has been added to the synthetic travel-time data used in the previous section. The random noise is normalized to 10% of the maximum travel-time differences, and it is added to the data to form the new data set shown in Figure 7a. Removing 40 degrees from each side of the data set in Figure 7a results in the reduced data shown in Figure 7b for 80-degree receiver-spanning arcs. The two-stage AR extrapolation technique is then applied to the data shown in Figure 7b to get the extended data from 80-degree spanning arcs to 160-degree spanning arcs. The resulting data are plotted in Figure 7c. The extended data in Figure 7c show the same overall pattern as the original noise-free data in Figure 5c even though the original data have noise added.

The data sets with noise added shown in Figure 7 are then used to do tomographic reconstructions. Figure 8a shows the inversion result using the original data in Figure 7a. Figure 8b is the inversion result using the partial data shown in Figure 7b. Figure 8c shows the reconstruction using the extended data in Figure 7c. Comparing the inversion results in Figure 8 and Figure 6, we see that the random noise adds many artificial fluctuations to the reconstructions and deforms the edges of the anomalies for the full data set (Figure 8a) and the partial data set (Figure 8b). Although the reconstruction with the extended data in Figure 8c also has some degradations compared to Figure 6c, the inversion is much cleaner than those with noisy partial and full data sets in Figure 8a and b and is much more consistent with the inversion in Figure 6c.

Real Data Testing

The AR extrapolation technique was then applied to real data recorded in the laboratory. The laboratory experiment had the same source–receiver geometry as the synthetic examples. The travel-time data were recorded by an oscilloscope and stored on the computer. The true model for this tomographic experiment is shown in Figure 9. The two squares are high-velocity heterogeneities with a velocity of about 2.65 km/s, and the background velocity is about 2 km/s. Figure 10a shows the travel-time differences between

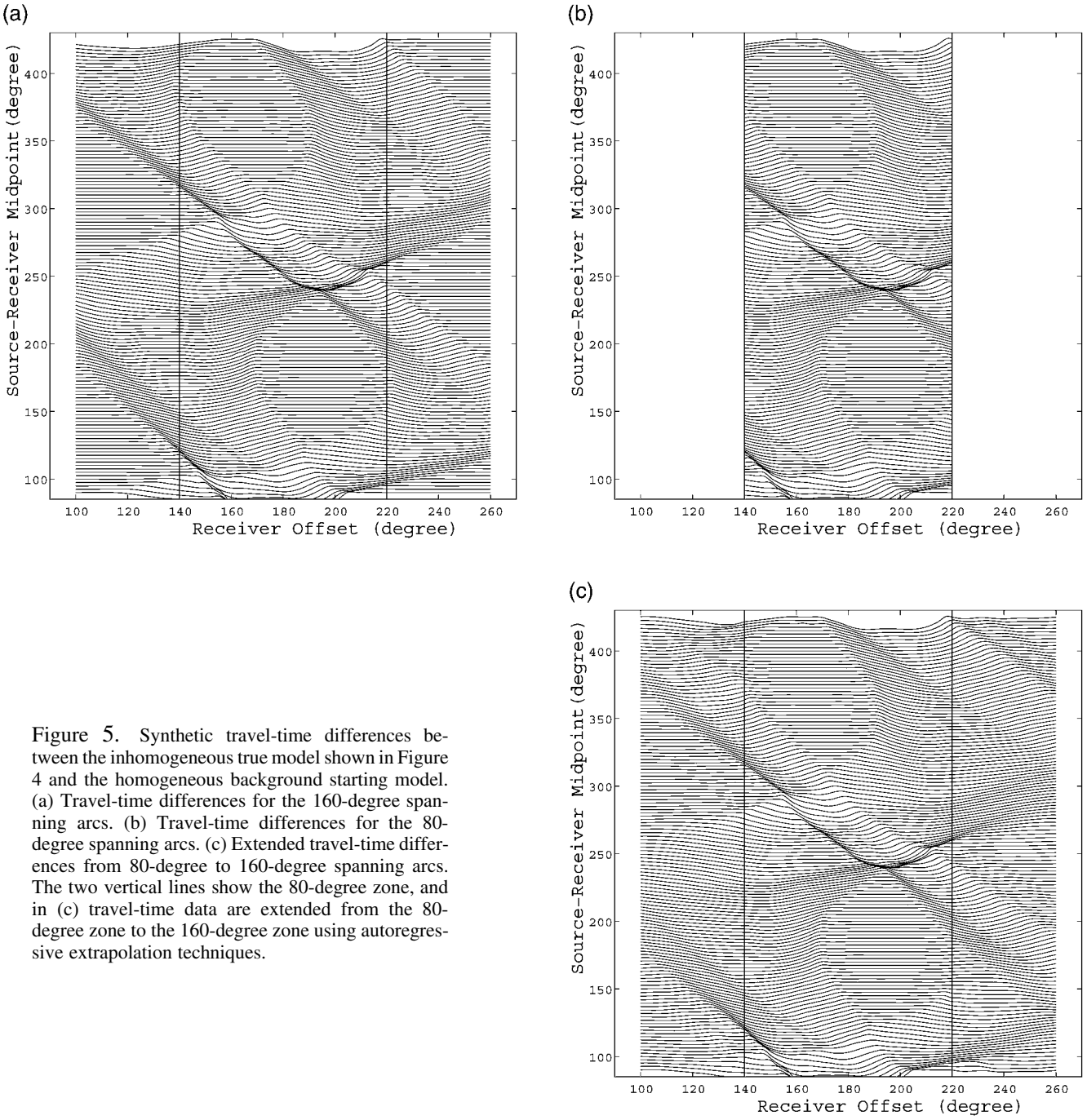

Figure 5. Synthetic travel-time differences between the inhomogeneous true model shown in Figure 4 and the homogeneous background starting model. (a) Travel-time differences for the 160-degree spanning arcs. (b) Travel-time differences for the 80-degree spanning arcs. (c) Extended travel-time differences from 80-degree to 160-degree spanning arcs. The two vertical lines show the 80-degree zone, and in (c) travel-time data are extended from the 80-degree zone to the 160-degree zone using autoregressive extrapolation techniques.

the manually picked travel times and the travel times for a homogeneous background starting model for the 160-degree case. To apply the AR extrapolation technique to this experimental data set, the original data were cut to a center spanning arc of 80 degrees to get a partial data set. The AR extrapolation technique was then applied to the partial data set and the extrapolated data set is shown in Figure 10b. In Figure 10b, data with a spanning arc less than 80 degrees remain the same as in the original data set in Figure 10a, whereas those data outside the range are extrapolated. Comparing Figures 10a and b, we can see that a similar overall pattern is seen in the original and extended data sets but the extrapolated data are smoother and more subdued.

The data sets shown in Figure 10 are used for tomographic reconstructions similar to those shown for the synthetic examples. Figure 11a shows the inversion result using the full data set in Figure 10a. Figure 11b shows the inversion result using the extrapolated data set in Figure 10b. Comparing Figure 11b to Figure 11a, we can see that the reconstruction using the extended data set is very close to the inversion using the full data set in Figure 10a. Moreover, Figure 11b shows a somewhat cleaner background velocity

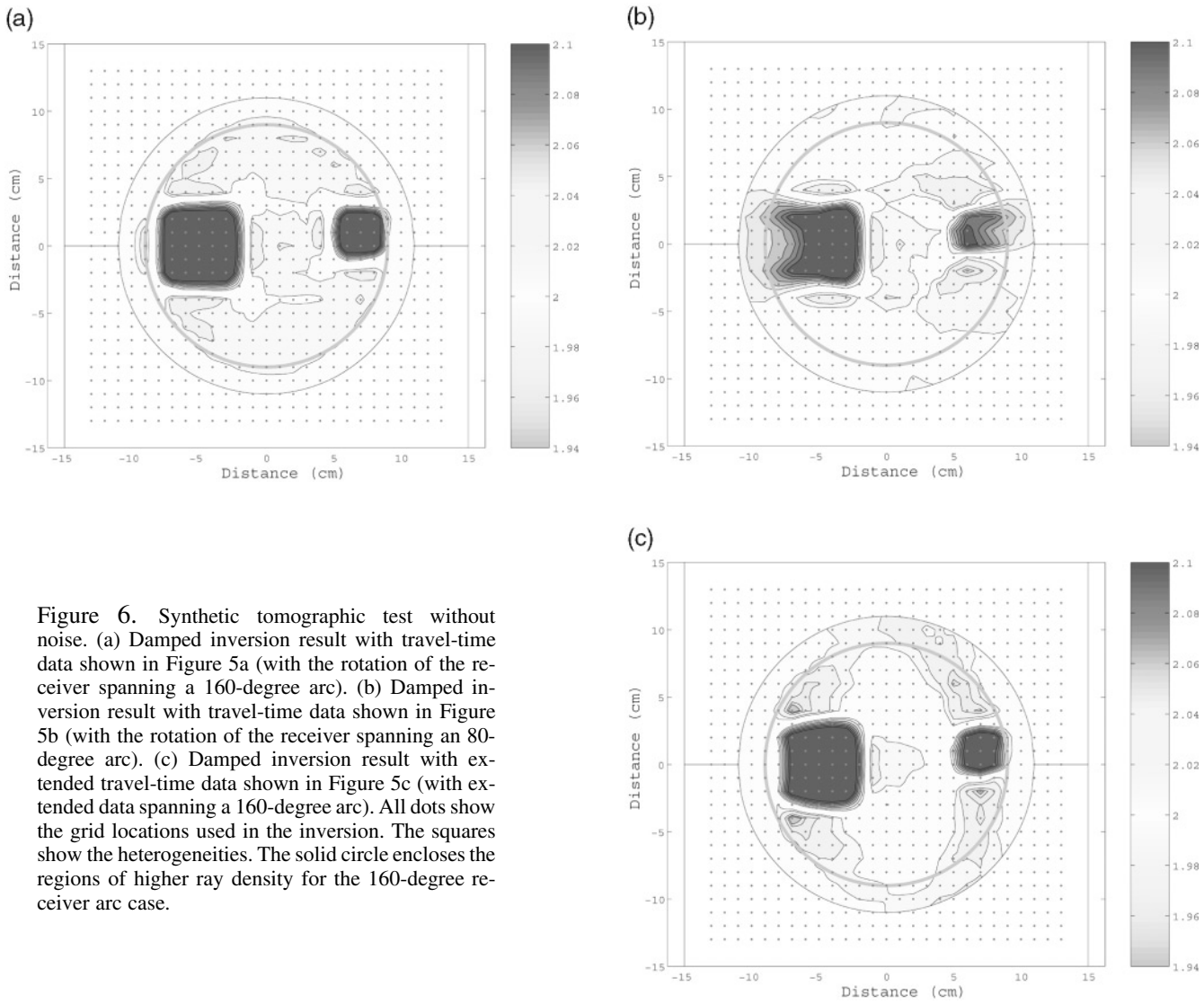

Figure 6. Synthetic tomographic test without noise. (a) Damped inversion result with travel-time data shown in Figure 5a (with the rotation of the receiver spanning a 160-degree arc). (b) Damped inversion result with travel-time data shown in Figure 5b (with the rotation of the receiver spanning an 80-degree arc). (c) Damped inversion result with extended travel-time data shown in Figure 5c (with extended data spanning a 160-degree arc). All dots show the grid locations used in the inversion. The squares show the heterogeneities. The solid circle encloses the regions of higher ray density for the 160-degree receiver arc case.

reconstruction than Figure 11a. This analysis confirms that the AR extrapolation technique can work for real laboratory data, which makes a further step toward its application to real data in the field.

Conclusions

Autoregressive extrapolation methods have been applied to the regularization of tomographic inversions using incomplete ray coverage. We used an experimental geometry for laboratory rock samples where full ray coverage is possible and then removed rays to obtain partial ray coverage. The tomographic applications show that the two-stage AR extrapolation technique is an effective way to perform data extrapolation for tomographic reconstructions. Both the synthetic tomographic applications with and without random noise and the real data example show that the two-stage AR extrapolation technique is a powerful tool for travel-time extrapolation and can improve the quality of tomographic reconstructions. Moreover, the two-stage AR extrapolation technique is tolerant to noise in the data and can still extrapolate the data to their original overall pattern, which is very important for real data extrapolation. Autoregressive extrapolation may also be very important for tomography experiments in the field since for these experiments complete ray coverage may be difficult to achieve. However, for data sets with too many missing values the performance of the AR extrapolation technique could be significantly degraded because there would not be enough known information available for the extrapolation process. In addition, although the AR extrapolation technique can tolerate and even remove random noise, coherent noise in real data applications may still be a problem.

Acknowledgments

The authors thank S. Fomel and an anonymous reviewer for their constructive reviews. The authors also thank L. Pyrak-Nolte for assistance in her rock physics laboratory.

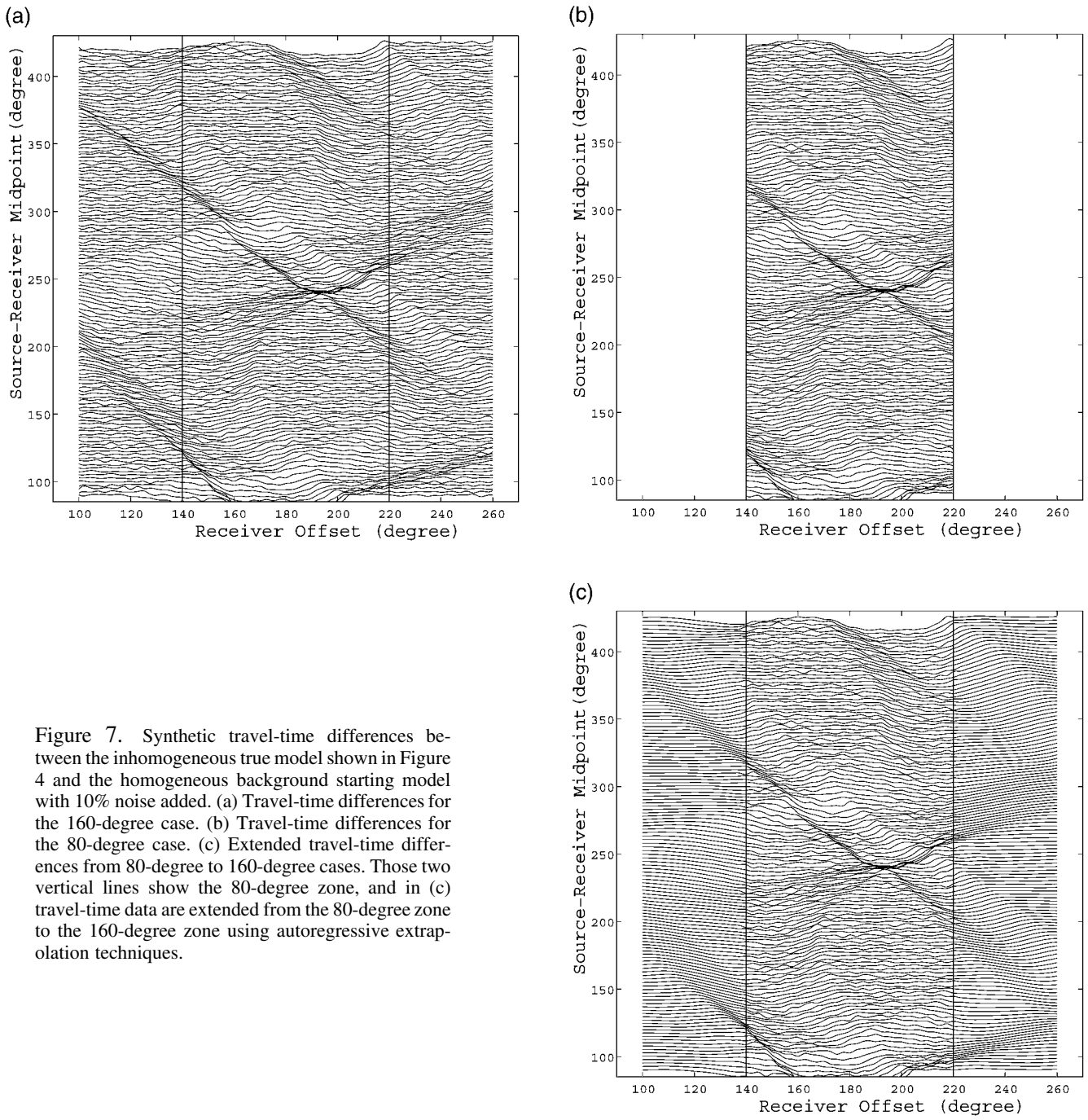

Figure 7. Synthetic travel-time differences between the inhomogeneous true model shown in Figure 4 and the homogeneous background starting model with 10% noise added. (a) Travel-time differences for the 160-degree case. (b) Travel-time differences for the 80-degree case. (c) Extended travel-time differences from 80-degree to 160-degree cases. Those two vertical lines show the 80-degree zone, and in (c) travel-time data are extended from the 80-degree zone to the 160-degree zone using autoregressive extrapolation techniques.

References

Burg, J. P. (1975). Maximum entropy spectral analysis, *Ph.D. Thesis*, Stanford University, http://sepwww.stanford.edu/theses/sep06 (last accessed March 2004).

Claerbout, J. F. (1992). *Earth Soundings Analysis: Processing versus Inversion*, Blackwell, Cambridge, Massachusetts.

Claerbout, J. F. (1998). Multidimensional recursive filters via a helix, *Geophysics* **63,** 1532–1541.

Claerbout, J. F. (2003). *Image Estimation by Example: Geophysical Soundings Image Construction: Multidimensional Autoregression*, web book, http://sepwww.stanford.edu/sep/prof/gee/toc_html (last accessed March 2004).

Fomel, S. (2003a). Theory of differential offset continuation, *Geophysics* **68,** 718–732.

Fomel, S. (2003b). Seismic reflection data interpolation with differential offset and shot continuation, *Geophysics* **68,** 733–744.

Fomel, S., and J. F. Claerbout (2003). Multidimensional recursive filter preconditioning in geophysical estimation problems, *Geophysics* **68,** 577–588.

Goodsill, S. J., and P. J. W. Rayner (1998). *Digital Audio Restoration*, Springer, New York.

Jain, A. K. (1989). *Fundamentals of Digital Image Processing*, Prentice Hall, Englewood Cliffs, New Jersey.

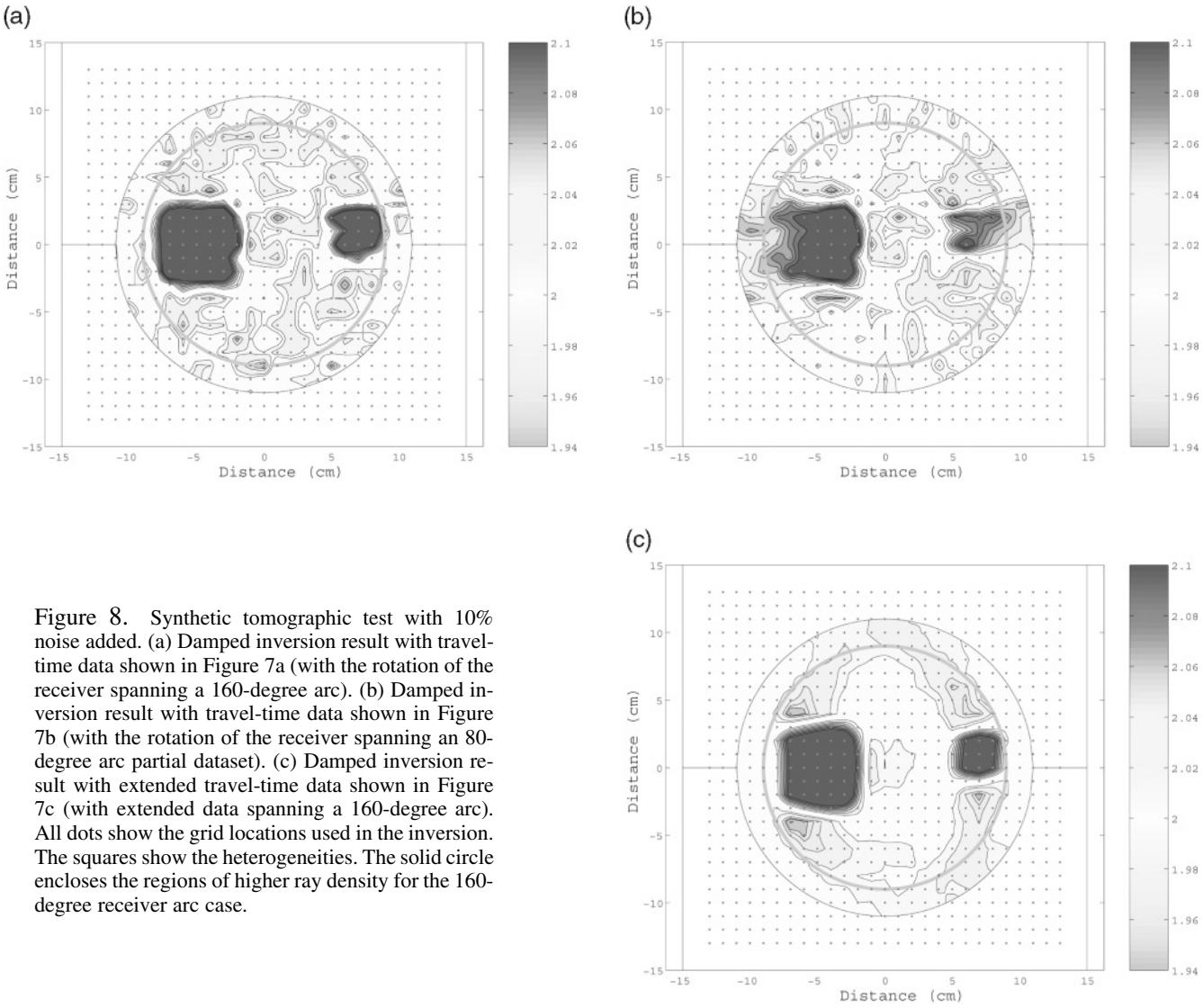

Figure 8. Synthetic tomographic test with 10% noise added. (a) Damped inversion result with travel-time data shown in Figure 7a (with the rotation of the receiver spanning a 160-degree arc). (b) Damped inversion result with travel-time data shown in Figure 7b (with the rotation of the receiver spanning an 80-degree arc partial dataset). (c) Damped inversion result with extended travel-time data shown in Figure 7c (with extended data spanning a 160-degree arc). All dots show the grid locations used in the inversion. The squares show the heterogeneities. The solid circle encloses the regions of higher ray density for the 160-degree receiver arc case.

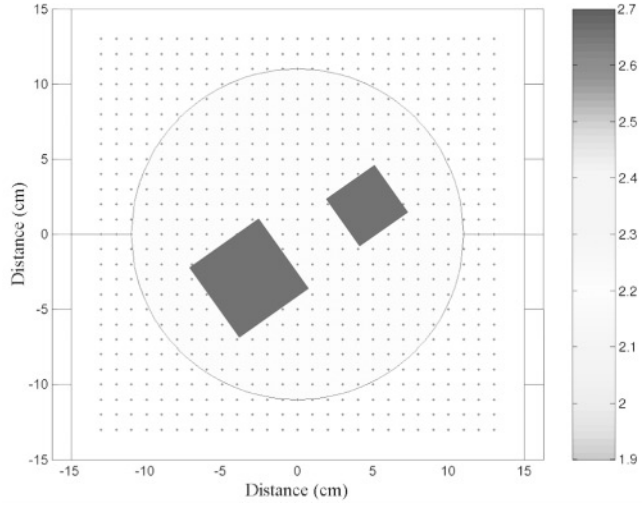

Figure 9. True model for laboratory experiment.

Tarantola, A. (1987). *Inverse Problem Theory*, Elsevier, Amsterdam.

VanDecar, J. C., and R. Snieder (1994). Obtaining smooth solutions to large, linear inverse problems, *Geophysics* **59,** 818–829.

Wang, B. (1993). Improvement of seismic travel-time inversion methods and application to observed data, *Ph.D. Thesis*, Purdue University, West Lafayette, Indiana.

Department of Earth and Atmospheric Sciences
550 Stadium Mall Drive
Purdue University
West Lafayette, Indiana 47907
lcpdq@purdue.edu
nowack@purdue.edu

Manuscript received 24 October 2003.

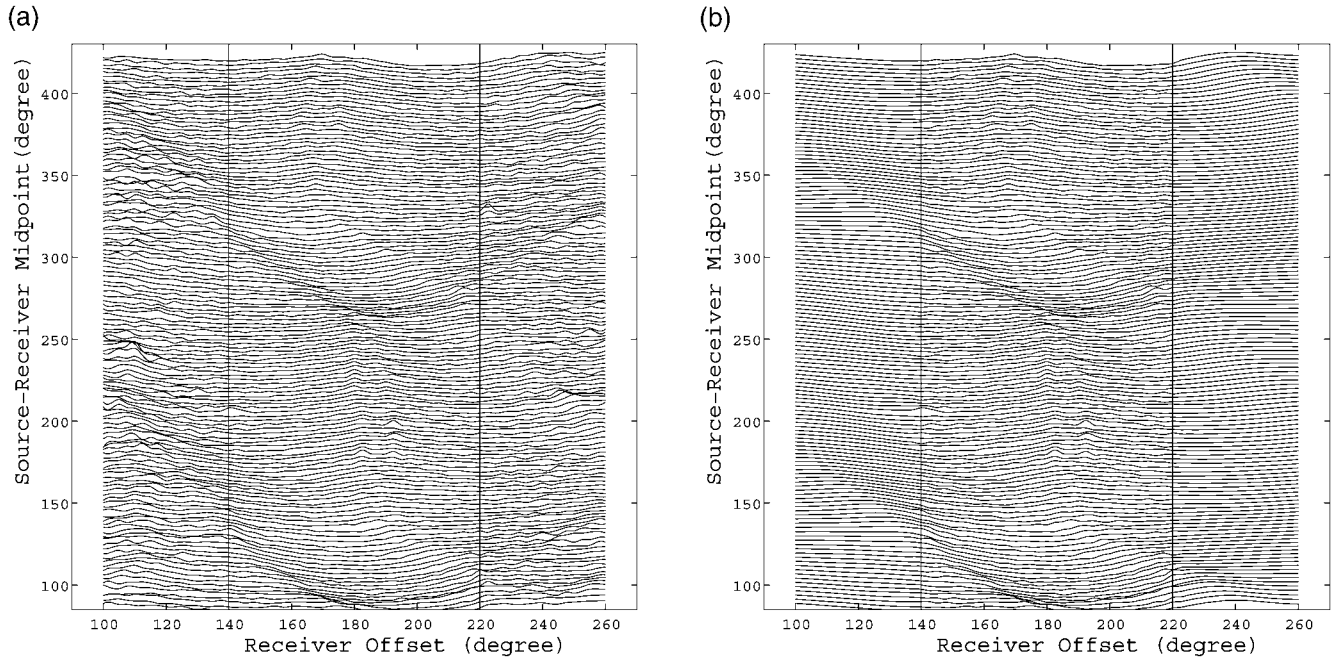

Figure 10. Observed experimental travel times. (a) Travel-time differences between the observed travel times from the model shown in Figure 9 and a homogeneous background starting model for the 160-degree spanning arcs. (b) Extended experimental travel-time differences from 80-degree to 160-degree spanning arcs.

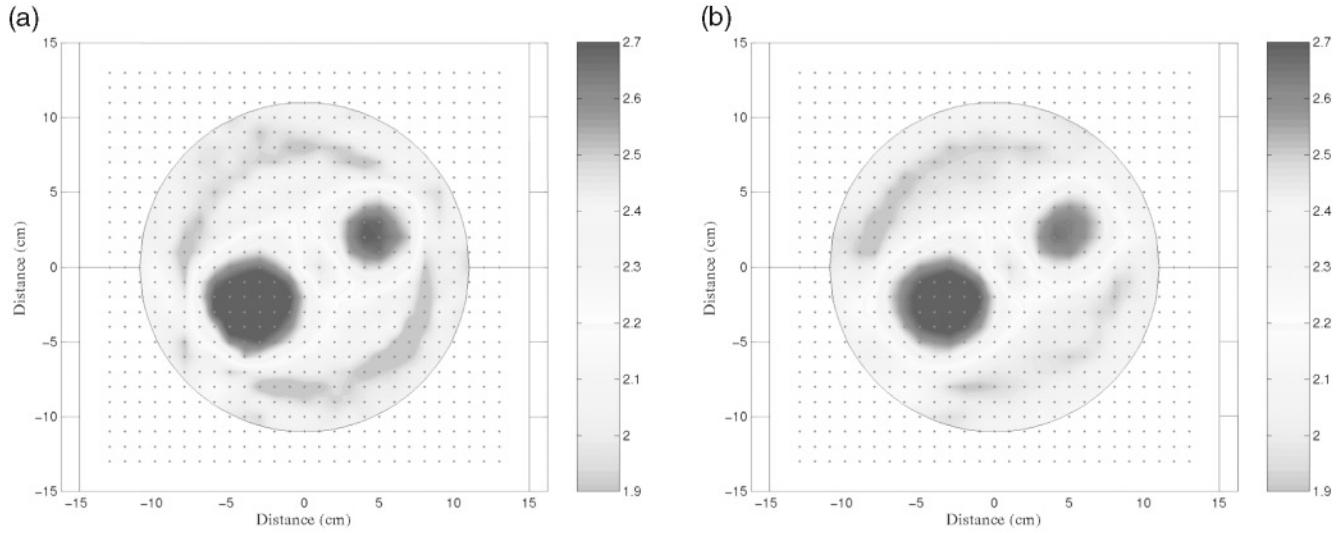

Figure 11. Tomographic reconstructions with observed laboratory data. (a) Inversion result with travel-time data shown in Figure 10a. (b) Inversion result with travel-time data shown in Figure 10b.